

Two dimensional vertically averaged and moment equations for rapidly varied flows

Les équations à deux dimensions en moyenne et moment sur la verticale pour les écoulements rapidement variables

HAITHAM K. GHAMRY, *Research Assistant, Ph.D., Dept. of Civil and Environmental Eng., University of Alberta, Edmonton, Alberta, Canada, T6G 2G7*

PETER M. STEFFLER, *MIAHR, Professor, Dept. of Civil and Environmental Eng., Univ. of Alberta, Edmonton, Alberta, Canada, T6G 2G7*

ABSTRACT

The classical depth averaged De St. Venant equations, which are used for most of the computational models in open channels, are based on the fundamental assumptions of uniform velocity and hydrostatic pressure distributions. They are thus limited in their applicability to cases where vertical details are not of importance. Alternative two-dimensional vertically averaged and moment equations are developed, by a moment weighted residual method from the fundamental 3D Reynolds equations, to account for problems where more vertical details are significant and essential. The proposed model is applied to rapidly varied flow problems involved in open channel flow. These problems include flow in channel transitions with rapid contraction and/or expansion and flow over a hemispherical hump. Linear distribution shapes are proposed for the horizontal velocity components, while quadratic distribution shapes are considered for vertical velocity and pressure. The implicit Petrov-Galerkin finite element scheme is used in these simulations. A good agreement is attained. In addition, the obtained results show that more details are gained and the flow is better represented by the proposed model compared to the classical De St. Venant model.

RÉSUMÉ

Les équations classiques de Saint-Venant moyennées sur la hauteur d'eau, qui sont utilisées dans la plupart des modèles numériques d'écoulements à surface libre, sont basées sur les hypothèses fondamentales de vitesse uniforme et de pression hydrostatique. Elles sont donc limitées dans leurs applications aux cas où les détails verticaux ont peu d'importance. Pour prendre en compte les problèmes dans lesquels les variations verticales sont significatives et essentielles, on a développé d'autres équations à deux dimensions en moyenne et moment sur la verticale; elles sont obtenues à partir des équations fondamentales de Reynolds tridimensionnelles par une méthode de résidus pondérés de moment. Ce modèle est appliqué à des problèmes d'écoulements rapidement variables en canal à surface libre comportant des rétrécissements et/ou élargissements brusques et passage au dessus d'une bosse hémisphérique. On adopte des profils linéaires pour les composantes horizontales de la vitesse, tandis que l'on considère des profils quadratiques pour la composante verticale et la pression. Ces simulations utilisent le schéma implicite en éléments finis de Petrov-Galerkin. On atteint un bon accord et les résultats obtenus montrent que l'on gagne plus de détails et que l'écoulement est mieux représenté par le modèle proposé que par le modèle classique de Saint-Venant.

Introduction

The derivation of De St. Venant equations is based on the assumptions of uniform velocity and hydrostatic pressure distributions. As a result, the previous equations are inapplicable for modeling flow situations that involve non-uniform velocity and/or non-hydrostatic pressure distributions and with length scales close to channel depth [20]. These flow situations include, for example, rapidly varied flows in hydraulic structures, sudden contractions and expansions and flow over bed form. These are important problems and require relatively accurate solutions in open channel hydraulics.

A number of attempts or approaches have been proposed in the past to model short length scale flow problems. Most of these attempts assumed that the flow could be approximated as potential flow in which vertical velocities and non-hydrostatic pressure distributions were used to predict the flow field. Kennedy [13] used a potential flow approximation to predict the flow field over dunes and antidunes. Dressler [1] introduced a bed curvilinear coordinate system into the Euler equations to come up with more general depth averaged equations. Boussinesq equations represent

the next level of approximation compared to the De St. Venant equations [5]. These equations assume linear vertical velocity and non-hydrostatic linear pressure distributions and are applicable for moderately shallow flows with wavelength to depth ratio of about six [20].

Steffler and Jin [20] introduced a further alternative in this area to recover more vertical details. They developed a new set of vertically averaged and moment equations. They derived the equations for the case of one-dimensional model in which they assumed a linear longitudinal velocity distribution, and quadratic vertical and pressure distributions. Successful numerical applications for that model were carried out by Khan [14]. Jin and Li [12] applied a one-dimensional model to solve problems where the effects of non-hydrostatic pressure distribution are significant. This model was considered as a simplification of the two-dimensional depth-averaged model derived by Jin and Steffler [11]. Naef [15] extended the model of Steffler and Jin [20] to a 2-D model. Ghamry [3] derived similar yet more general equations to those of Naef [15] to account for problems where more vertical details are significant and essential. The new two-dimensional vertically averaged and moment (termed VAM) equations were

Revision received January 24, 2002. Open for discussion till February 28, 2003.

derived by a moment weighted residual method from the fundamental three-dimensional Reynolds equations. The equations were developed in a general way that can accommodate different shapes of velocity and pressure distributions. The derivation of the new equations could be considered as a quasi three-dimensional model where more vertical details are accounted for, without extending to the full three-dimensional Navier Stokes equations.

Among others, an attempt to apply a three-dimensional model to curved open channels was carried out by Shimuzi et al. [19]. Odgaard et al. [16] developed a three-dimensional model for simulating flow through natural river reaches. The model solved the Reynolds averaged Navier Stokes equations.

The main goals of this paper are: 1) to test the proposed VAM model for simulating rapidly varied flow situations with relatively small wavelength to depth ratios ($\lambda/h \approx 5$, λ being the wavelength) where non-hydrostatic pressure and non-uniform velocity distributions might be expected to be significant; and 2) to see if there is an improvement of the proposed model over the conventional De St. Venant (termed VA) model in simulating such flows.

Mathematical and Numerical Model

The vertically averaged and moment equations developed by Ghamry [3] are adapted to allow for the incorporation of pre-assumed linear distribution of horizontal velocity components and quadratic vertical velocity and pressure distributions. The distribution shapes proposed to the velocities as well as pressure are as follows:

The proposed linear horizontal velocity distributions read

$$u = u_o + u_1(2\eta - 1) \quad (1)$$

$$v = v_o + v_1(2\eta - 1) \quad (2)$$

where u is the longitudinal velocity; v is the transverse velocity; and η is the non-dimensional vertical coordinate and is defined as

$$\eta = (z - z_b) / h \quad (3)$$

where z_b is the bed elevation; and h is the depth of flow. In both cases $\int_0^1 (2\eta - 1) d\eta = 0$ and $(2\eta - 1)_{\eta=1} = 1$ so that u_o and v_o are the

depth averaged velocity components and u_1 and v_1 can be interpreted as the velocities at the water surface in excess of the means u_o and v_o respectively. These excess surface velocities do not contribute to net mass flux. The proposed vertical velocity distribution reads

$$w = w_b(1 - \eta) + w_2 4\eta(1 - \eta) + w_h \eta \quad (4)$$

where w is the vertical velocity; w_b is the vertical velocity at the bed; w_h is the vertical velocity at the surface; and w_2 is the mid-depth vertical velocity in excess of the average of vertical velocities at the surface and bed. The vertical velocity at the bed, w_b , is given by the following kinematic bed boundary condition:

$$w_b = (u_o - u_1) \frac{\partial z_b}{\partial x} + (v_o - v_1) \frac{\partial z_b}{\partial y} \quad (5)$$

This condition assumes that the bed stays fixed with time and the flow is parallel to the bed. The surface vertical velocity w_h is given by the following kinematic surface condition:

$$w_h = \frac{\partial h}{\partial t} + (u_o + u_1) \frac{\partial}{\partial x} (h + z_b) + (v_o + v_1) \frac{\partial}{\partial y} (h + z_b) \quad (6)$$

The proposed pressure distribution reads

$$p = \rho g (h + h_1) (1 - \eta) + \rho g h_2 4\eta (1 - \eta) \quad (7)$$

where p is the pressure; ρ is the density of water; and g is the acceleration due to gravity. h_1 is the pressure head in excess of the hydrostatic at the bed and is equal to $p_1/\rho g$, p_1 being the pressure intensity in excess of the hydrostatic at bed. h_2 is the mid-depth pressure head in excess of the average of pressure heads at the bed and surface and is equal to $p_2/\rho g$, p_2 being the mid-depth pressure in excess of the average of pressures at the bed and surface.

At the water surface, the pressure is assumed atmospheric and turbulent shear and normal stresses are assumed negligible [20]. Having applied the previous proposed distributions along with the kinematic and surface boundary conditions, we are left with the following equations:

The vertically averaged continuity equation

$$\frac{\partial h}{\partial t} + \frac{\partial q_x}{\partial x} + \frac{\partial q_y}{\partial y} = 0 \quad (8)$$

The vertically averaged momentum equation in the x -direction

$$\begin{aligned} \frac{\partial q_x}{\partial t} + \frac{\partial}{\partial x} \left(\frac{q_x^2}{h} \right) + \frac{\partial}{\partial y} \left(\frac{q_x q_y}{h} \right) + \frac{1}{3} \left(\frac{\partial h u_1^2}{\partial x} + \frac{\partial h u_1 v_1}{\partial y} \right) + \\ gh \frac{\partial}{\partial x} (h + z_b) + \frac{g}{2} \frac{\partial h h_1}{\partial x} + \frac{2g}{3} \frac{\partial h h_2}{\partial x} + g h_1 \frac{\partial z_b}{\partial x} - \\ \frac{1}{\rho} \frac{\partial h \bar{\sigma}_x}{\partial x} - \frac{1}{\rho} \frac{\partial h \bar{\tau}_{xy}}{\partial y} + \frac{1}{\rho} \tau_{xz_b} = 0 \end{aligned} \quad (9)$$

The vertically averaged momentum equation in the y -direction

$$\begin{aligned} \frac{\partial q_y}{\partial t} + \frac{\partial}{\partial x} \left(\frac{q_y q_x}{h} \right) + \frac{\partial}{\partial y} \left(\frac{q_y^2}{h} \right) + \frac{1}{3} \left(\frac{\partial h v_1^2}{\partial y} + \frac{\partial h u_1 v_1}{\partial x} \right) + \\ gh \frac{\partial}{\partial y} (h + z_b) + \frac{g}{2} \frac{\partial h h_1}{\partial y} + \frac{2g}{3} \frac{\partial h h_2}{\partial y} + g h_1 \frac{\partial z_b}{\partial y} - \\ \frac{1}{\rho} \frac{\partial h \bar{\sigma}_y}{\partial y} - \frac{1}{\rho} \frac{\partial h \bar{\tau}_{yx}}{\partial x} + \frac{1}{\rho} \tau_{yz_b} = 0 \end{aligned} \quad (10)$$

The vertically averaged momentum equation in the z -direction

$$\begin{aligned} \frac{\partial h \bar{w}}{\partial t} + \frac{\partial \bar{w} q_x}{\partial x} + \frac{\partial \bar{w} q_y}{\partial y} - \frac{1}{6} \frac{\partial}{\partial x} [h u_1 (w_b - w_h)] - \\ \frac{1}{6} \frac{\partial}{\partial y} [h v_1 (w_b - w_h)] - \frac{1}{\rho} \frac{\partial h \bar{\tau}_{zx}}{\partial x} - \frac{1}{\rho} \frac{\partial h \bar{\tau}_{zy}}{\partial y} - \\ gh_1 - \frac{1}{\rho} \tau_{yz_b} \frac{\partial z_b}{\partial y} - \frac{1}{\rho} \tau_{xz_b} \frac{\partial z_b}{\partial x} = 0 \end{aligned} \quad (11)$$

The moment of continuity equation

$$\frac{1}{4} \frac{\partial h^2}{\partial t} + \frac{1}{6} \left(\frac{\partial h^2 u_1}{\partial x} + \frac{\partial h^2 v_1}{\partial y} \right) + q_x \frac{\partial \bar{z}}{\partial x} + q_y \frac{\partial \bar{z}}{\partial y} - h \bar{w} = 0 \quad (12)$$

The moment of momentum equation in the x -direction

$$\begin{aligned} & \frac{\partial u_1}{\partial t} + \frac{\partial}{\partial x} \left(\frac{q_x u_1}{h} \right) + v_1 \frac{\partial}{\partial y} \left(\frac{q_x}{h} \right) + \frac{q_y}{h} \frac{\partial u_1}{\partial y} + \\ & \left[\frac{gh_1}{3h} \frac{\partial h}{\partial x} - \frac{g}{3} \frac{\partial h_1}{\partial x} + \frac{8gh_2}{3h} \frac{\partial \bar{z}}{\partial x} - \frac{4\bar{\sigma}_x}{hp} \frac{\partial \bar{z}}{\partial x} - \right. \\ & \left. \frac{3}{2} \left(\frac{4\bar{\tau}_{xy}}{hp} \frac{\partial \bar{z}}{\partial y} + \frac{4\bar{\tau}_{xz}}{hp} - \frac{2}{hp} \tau_{xz_b} \right) \right] = 0 \end{aligned} \quad (13)$$

The moment of momentum equation in the y -direction

$$\begin{aligned} & \frac{\partial v_1}{\partial t} + \frac{\partial}{\partial y} \left(\frac{q_y v_1}{h} \right) + u_1 \frac{\partial}{\partial x} \left(\frac{q_y}{h} \right) + \frac{q_x}{h} \frac{\partial v_1}{\partial x} + \\ & \left[\frac{gh_1}{3h} \frac{\partial h}{\partial y} - \frac{g}{3} \frac{\partial h_1}{\partial y} + \frac{8gh_2}{3h} \frac{\partial \bar{z}}{\partial y} - \frac{4\bar{\sigma}_y}{hp} \frac{\partial \bar{z}}{\partial y} - \right. \\ & \left. \frac{3}{2} \left(\frac{4\bar{\tau}_{yx}}{hp} \frac{\partial \bar{z}}{\partial x} + \frac{4\bar{\tau}_{yz}}{hp} - \frac{2}{hp} \tau_{yz_b} \right) \right] = 0 \end{aligned} \quad (14)$$

The moment of momentum equation in the z -direction

$$\begin{aligned} & \frac{\bar{w}}{4} \frac{\partial h^2}{\partial t} - \frac{\partial}{\partial t} \left[\frac{h^2}{12} (w_b - w_h) \right] - h \bar{w}^2 + \left[q_x \bar{w} - \frac{h u_1}{6} (w_b - w_h) \right] \\ & \frac{\partial \bar{z}}{\partial x} + \left[q_y \bar{w} - \frac{h v_1}{6} (w_b - w_h) \right] \frac{\partial \bar{z}}{\partial y} - \frac{\partial}{\partial x} \left[\frac{h q_x}{12} (w_b - w_h) \right] - \\ & \frac{\partial}{\partial y} \left[\frac{h q_y}{12} (w_b - w_h) \right] + \frac{\partial}{\partial x} \left[\frac{h^2 u_1}{10} \frac{2}{3} \left(\frac{3}{2} \bar{w} + \frac{w_b}{2} + \frac{w_h}{2} \right) \right] + \\ & \frac{\partial}{\partial y} \left[\frac{h^2 v_1}{10} \frac{2}{3} \left(\frac{3}{2} \bar{w} + \frac{w_b}{2} + \frac{w_h}{2} \right) \right] - \frac{h}{\rho} \left(\bar{\tau}_{zx} \frac{\partial \bar{z}}{\partial x} + \bar{\tau}_{zy} \frac{\partial \bar{z}}{\partial y} - \bar{\sigma}_x \right) + \\ & \frac{h}{2\rho} \tau_{yz_b} \frac{\partial z_b}{\partial y} + \frac{h}{2\rho} \tau_{xz_b} \frac{\partial z_b}{\partial x} - \frac{2g}{3} h_2 = 0 \end{aligned} \quad (15)$$

where q_x is the flow discharge in longitudinal direction per unit width; q_y is the flow discharge in transverse direction per unit width; \bar{z} is the mid channel depth; $\bar{\tau}$ is the vertically averaged total turbulent shear stress; τ is the bed shear stress; and σ is the total turbulent normal stress. The average vertical velocity, \bar{w} , and the mean square vertical velocity, \bar{w}^2 , are given by

$$\bar{w} = \frac{1}{2} w_b + \frac{2}{3} w_2 + \frac{1}{2} w_h \quad (16)$$

$$\bar{w}^2 = \bar{w}^2 + \frac{w_b^2}{12} + \frac{w_h^2}{12} - \frac{w_b w_h}{6} + \frac{1}{20} (2\bar{w} - w_b - w_h)^2 \quad (17)$$

The above set of equations ((5)-(6) and (8)-(15)) is called in this paper the VAM model. It should be mentioned that these derived equations are identical to those obtained by Naef [15]. The vertically averaged total turbulent shear and normal stresses appearing in equations (9)-(11) and (13)-(15) are approximated (assuming laminar stresses are negligible) according to the Boussinesq model as follows:

$$\bar{\sigma}_x = \bar{\tau}_{xx} = \frac{1}{h} \int_{z_b}^{z_b+h} \tau_{xx} = 2\rho v_h \frac{\partial}{\partial x} \left(\frac{q_x}{h} \right) \quad (18)$$

$$\bar{\sigma}_y = \bar{\tau}_{yy} = \frac{1}{h} \int_{z_b}^{z_b+h} \tau_{yy} = 2\rho v_h \frac{\partial}{\partial y} \left(\frac{q_y}{h} \right) \quad (19)$$

$$\bar{\sigma}_z = \bar{\tau}_{zz} = \frac{1}{h} \int_{z_b}^{z_b+h} \tau_{zz} = 2\rho v_z \frac{\partial \bar{w}}{\partial z} = 2\rho v_z \frac{w_h - w_b}{h} \quad (20)$$

$$\bar{\tau}_{xy} = \bar{\tau}_{yx} = \frac{1}{h} \int_{z_b}^{z_b+h} \tau_{yx} = \rho v_h \left[\frac{\partial}{\partial y} \left(\frac{q_x}{h} \right) + \frac{\partial}{\partial x} \left(\frac{q_y}{h} \right) \right] \quad (21)$$

$$\bar{\tau}_{xz} = \bar{\tau}_{zx} = \frac{1}{h} \int_{z_b}^{z_b+h} \tau_{zx} = \rho v_z \left(\frac{\partial \bar{u}}{\partial z} + \frac{\partial \bar{w}}{\partial x} \right) = \rho v_z \left(2 \frac{u_1}{h} + \frac{\partial \bar{w}}{\partial x} \right) \quad (22)$$

$$\bar{\tau}_{yz} = \bar{\tau}_{zy} = \frac{1}{h} \int_{z_b}^{z_b+h} \tau_{yz} = \rho v_z \left(\frac{\partial \bar{v}}{\partial z} + \frac{\partial \bar{w}}{\partial y} \right) = \rho v_z \left(2 \frac{v_1}{h} + \frac{\partial \bar{w}}{\partial y} \right) \quad (23)$$

where v_h is the vertically averaged turbulent exchange coefficient or eddy viscosity in the horizontal direction (x - y plane); and v_z is the vertically averaged turbulent eddy viscosity in the vertical direction. For simplicity, the case of bed-dominated turbulence is assumed and values of the order of $v_h = 0.5u_*h$ and $v_z = 0.07u_*h$ are used [2]. u_* is the shear velocity and is defined as

$$u_* = \sqrt[4]{\left(\frac{\tau_{xz_b}}{\rho} \right)^2 + \left(\frac{\tau_{yz_b}}{\rho} \right)^2} \quad (24)$$

It should be mentioned, herein, that the present proposed models for turbulent shear stresses represent the simplest models available. More sophisticated models are possible and their incorporation may be an interesting topic for further research.

The bed shear stresses, appearing in equations (9)-(11) and (13)-(15), are approximated according to

$$\tau_{xz_b} = \frac{\rho}{C_*^2} u_o \sqrt{u_o^2 + v_o^2 + \bar{w}^2} \quad (25)$$

$$\tau_{yz_b} = \frac{\rho}{C_*^2} v_o \sqrt{u_o^2 + v_o^2 + \bar{w}^2} \quad (26)$$

where C_* is the dimensionless Chezy Coefficient and is related to the effective roughness height, k_s , through

$$C_* = 5.75 \log \left(12 \frac{h}{k_s} \right) \quad (27)$$

Boundary Conditions

The mathematical character of this set of equations has not yet been studied, and as a result, definitive boundary and initial condition requirements have not been established. For practical purposes, the following approach to boundary conditions seems to work: the continuity and horizontal momentum equations are essentially the shallow water equations and use the appropriate set of boundary conditions for sub- and supercritical inflow and outflow and no flow cases. For the case of subcritical flow, a given total flow is specified at the upstream cross-section as an inflow boundary, whereas a fixed water surface elevation is specified at

the downstream cross-section as an outflow boundary. For case of supercritical flow, both the flow and the water surface elevation are given at the upstream cross-section as inflow conditions, whereas no conditions are applied at the outflow boundary. A no cross-flow condition is specified at any vertical wall boundaries. The equations of moment of horizontal momentum appear to have the characteristic of transport equations. As a result, values for the velocities in excess of the means at the surface, u_I and v_I , are given at the upstream cross-section for inflow boundary case, whereas they are left free at the outflow boundary case. It is found that assuming constant definite values other than zero for u_I and v_I at the inflow boundary does not affect the output results. This arises from the fact that the upstream boundary is placed sufficiently far upstream of the domain of interest that the flow becomes fully developed by the time the domain of interest is reached. For the sake of simplicity, u_I and v_I are assumed to be zero as boundary conditions at the upstream boundary. At the walls, a slip velocity condition is specified for u_I and v_I . That means the velocities in excess of the means at the surface, u_I and v_I , may have a component parallel to the wall, but not perpendicular to the wall. In the rest of the equations, the primary dependent variable being evaluated is not differentiated with respect to the spatial coordinates. As a result, the variables \bar{w} or w_2 , w_b , w_h , p_I , and p_2 are left free at all boundaries. At time $t = 0$, all variables are defined to have initial values at each point of the domain of interest.

Having defined the initial values of the variables and specified the boundary conditions, we are left with a closed system that defines a 'model' for 2-D or a quasi 3-D flow in open channels (equations (5)-(6) and (8)-(15)). This model, essentially, solves for " w_b ", " w_h ", " h ", " q_x ", " q_y ", " p_I or h_I ", " \bar{w} or w_2 ", " u_I ", " v_I ", and " p_2 or h_2 " dependent variables respectively. This results in a ten-equation by a ten-unknown (10 x 10) model (the VAM model). If we force h_I , \bar{w} , u_I and v_I , and h_2 to zero and eliminate their corresponding equations ((11), (12) and (13)-(15)), then we'll be left with a three-equation by a three-unknown (3x3) model. This model (equations (8)-(10)) is the traditional De St. Venant or VA model. These equations were used in most of the applications of this paper to compare their results with those of the proposed VAM equations.

Numerical Solution of the Equations

A numerical solution is necessary since there is no feasible analytical solution. The finite element method is used in this paper. The vertically averaged and moment equations are discretized and modeled using a hybrid Petrov-Galerkin and Standard-Galerkin finite element scheme. The vertically averaged continuity, longitudinal and transverse momentum, and moment of longitudinal and transverse momentum equations are upwinded using the two-dimensional Characteristic Dissipative Galerkin finite element scheme recently used by Ghanem et al. [4]. This scheme has the ability of providing selective artificial dissipation for shock capturing and modeling both progressive and regressive waves accurately ([6], [7], and [4]). The rest of the equations are modeled using the Standard-Galerkin finite element scheme. This may be

briefly explained as follows:

The application of the Petrov-Galerkin (Streamline Upwind) finite element scheme to equations (8)-(10) and (13)-(14) results in the following weak statement equation:

$$\int_{\Omega} \hat{\mathbf{B}} \left(\frac{\partial \boldsymbol{\Psi}(\tilde{\Phi})}{\partial t} + \frac{\partial \mathbf{F}_x(\tilde{\Phi})}{\partial x} + \frac{\partial \mathbf{F}_y(\tilde{\Phi})}{\partial y} + \mathbf{G}(\tilde{\Phi}) \right) d\Omega = 0 \quad (28)$$

where bold letters represent vectors and matrices. $\boldsymbol{\Psi}(\tilde{\Phi})$ represents the time-variation vector. $\mathbf{F}_x(\tilde{\Phi})$ and $\mathbf{F}_y(\tilde{\Phi})$ represent the flux vectors in the x - and y -directions respectively. $\mathbf{G}(\tilde{\Phi})$ represents the sink and/or source vector. Ω is the solution domain. The approximation, $\tilde{\Phi}$, to the unknown vector, Φ , is defined as

$$\tilde{\Phi} = \mathbf{B}^T \Phi \quad (29)$$

where Φ is the nodal-value vector of the unknowns; and \mathbf{B} is the matrix of basis functions (triangular elements with linear basis functions for all variables are used).

$$\hat{\mathbf{B}} = \mathbf{B} + \omega \Delta x \mathbf{W}_x \frac{\partial \mathbf{B}}{\partial x} + \omega \Delta y \mathbf{W}_y \frac{\partial \mathbf{B}}{\partial y} \quad (30)$$

$\hat{\mathbf{B}}$ is the matrix of test functions. ω is an upwinding coefficient set equal to 0.5 for this study. \mathbf{W}_x and \mathbf{W}_y are the upwinding matrix coefficients in x and y directions respectively which control both the amount and the direction of the numerical diffusion. The upwinding matrices, \mathbf{W}_x and \mathbf{W}_y , are calculated according to Hughes and Mallet ([8] and [9]) and Hughes et al. [10]. It should be emphasized that more details regarding Petrov-Galerkin scheme can be found in [7].

The application of the Standard-Galerkin Scheme to the rest of the equations results in the following weak statement equation

$$\int_{\Omega} \mathbf{B} \left(\frac{\partial \boldsymbol{\Psi}(\tilde{\Phi})}{\partial t} + \frac{\partial \mathbf{F}_x(\tilde{\Phi})}{\partial x} + \frac{\partial \mathbf{F}_y(\tilde{\Phi})}{\partial y} + \mathbf{G}(\tilde{\Phi}) \right) d\Omega = 0 \quad (31)$$

Applications

Comparisons of the model predictions are made with the experimental results obtained by Ye and McCorquodale [21], and Shamloo and Rajaratnam [18]. These channels are selected as they have relatively small wavelength to depth ratios ($\lambda/h \approx 5$) where non-hydrostatic pressure and non-uniform velocity distributions might be expected to be significant. As a result, a noticeable difference between the proposed model and the conventional De St. Venant model could be anticipated.

In all cases, the finite element grids are designed to be fine enough to meet the requirements of reasonable accuracy as well as execution time. In addition, additional nodes are added to the parts of the computational domain where velocity gradients are expected to be high, while fewer nodes are placed in the other parts of the flume where lesser velocity gradients are expected. The program is run till a steady state solution is obtained.

Ye and McCorquodale's [21] experiment

The flume results of Ye and McCorquodale [21] are invoked to test the ability of the model to simulate nearly critical flow conditions. The experiment was conducted at the University of Windsor in a Parshall flume. The Parshall flume, which was developed by Parshall [17], is considered one of the most widely installed open channel devices for field flow measurements. The flume consisted of a contracting section with a flat floor to create the critical depth; a throat section with parallel side walls and a sloping bed in which supercritical flow occurs; and a diverging section with an adverse sloping bed. The flume had a rectangular cross section. The flow discharge was equal to $0.0145 \text{ m}^3/\text{s}$.

The simulation is performed using a finite element mesh composed of 2485 triangular elements and 1383 nodes (Figure 1). The boundary conditions are specified as subcritical inflow, supercritical outflow and no-flow across the side vertical walls. The boundary condition specified at the inflow section is a total discharge = $0.0145 \text{ m}^3/\text{s}$.

The results are shown in Figures 2-4. Figure 2 compares the experimental and numerically predicted cross channel averaged water surface elevation. Figures 3-4 compare the experimental and numerically predicted depth averaged longitudinal velocity distributions across the flume at different cross sections.

It can be clearly seen from Figure 2 that the proposed VAM model simulates well the cross channel averaged water surface elevation. In addition, the proposed model predicts the flow slightly better than the traditional De St. Venant model in the vicinity of the critical flow section.

It can be noticed from Figures 3-4 that the agreement with the experimental results is generally good. The model underestimates the results particularly near the walls at some cross sections (cross sections 3, 4 and 7). In addition, the VAM and De St. Venant (VA) models seem to behave almost the same. This is to be expected as the ratio of the wavelength to depth is relatively moderate for this problem. Thus, the effect of the non-hydrostatic pressure and non-uniform velocity distributions might not be expected to be significant.

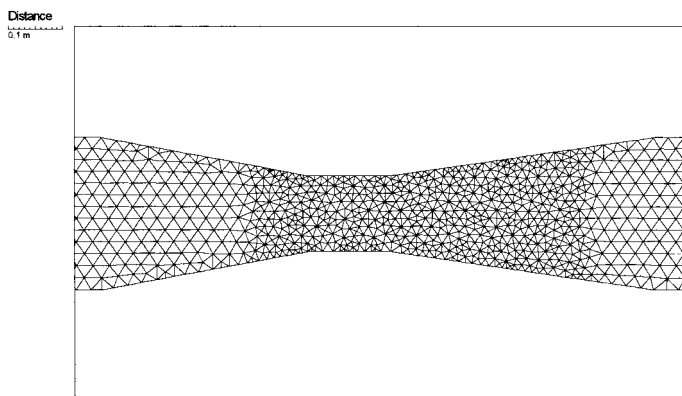


Fig. 1 Finite element mesh for Ye and McCorquodale's (1997) experiment

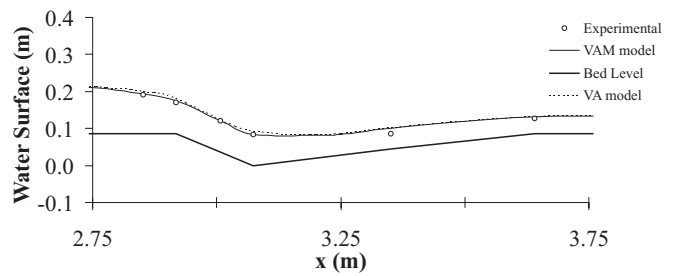


Fig. 2 The comparison of cross channel averaged surface elevation for Ye and McCorquodale's (1997) experiment

Shamloo and Rajaratnam's [18] experiment

One of the flume results of Shamloo and Rajaratnam [18] is used to test the ability of the model to simulate rapidly varied flow over a hump where the flow exhibits three-dimensional characteristics. The flume was 18 m long, 1.22 m wide and 0.65 m high. The bed was non-erodible, made of smooth aluminum, with Plexiglas side walls. The flume had an adjustable bed slope and a tailgate to control the downstream flow depth.

Measurements of the water surface profiles, velocity and shear stress were presented. The water surface profiles were measured by point gauges. The velocities were measured by pitot-static tube

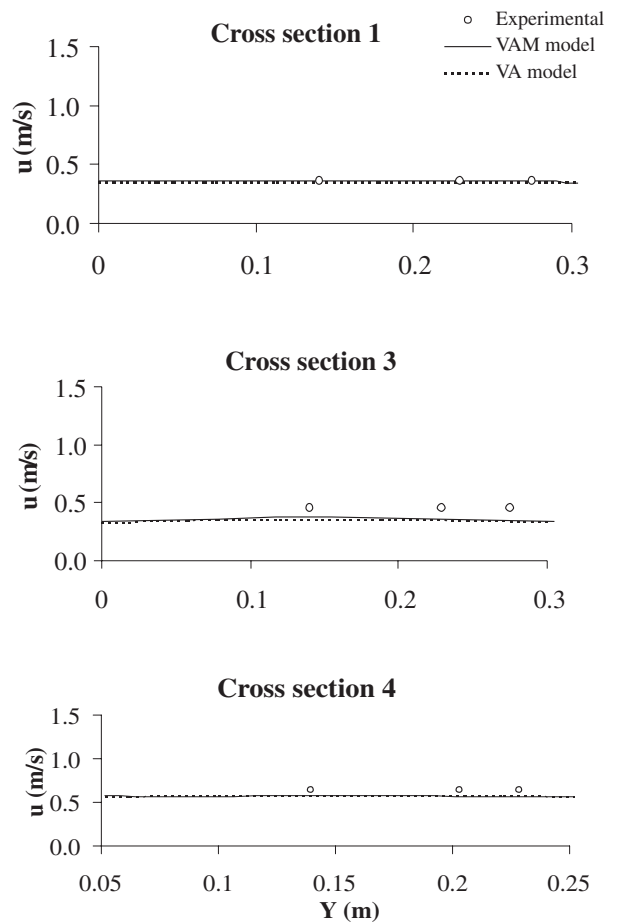


Fig. 3 The comparison of longitudinal velocity distribution across the flume for Ye and McCorquodale's (1997) experiment (cross sections 1, 3 and 4)

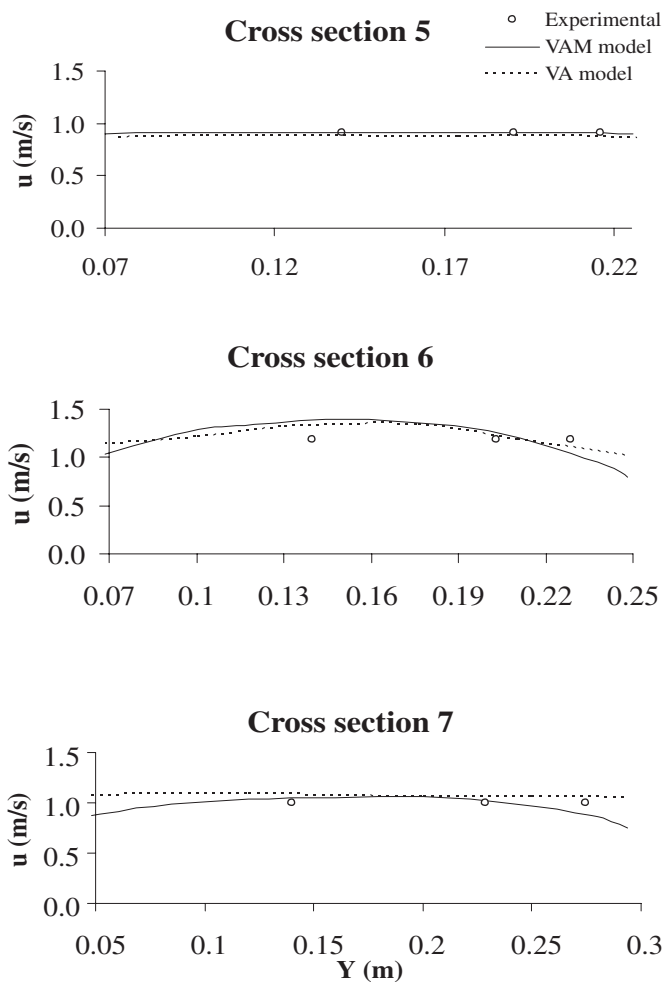


Fig. 4 The comparison of longitudinal velocity distribution across the flume for Ye and McCorquodale's (1997) experiment (cross sections 5, 6 and 7)

in uni-directional flow and by yaw and pitch probes in two-dimensional flows. A smooth bed was used for the velocity field measurements, with a simple Styrofoam hemisphere (of sizes 74 and 134 mm in diameter) glued on the aluminum bed. The uncertainty in the water surface and velocity measurements were ± 1.00 mm and ± 0.0064 m/s respectively. Experimental velocities below the pressure transducer range were not recorded. The maximum flow rate was about $0.075 \text{ m}^3/\text{s}$. A number of experiments were conducted for different flow conditions, with different obstacles and bed roughnesses. The experiment with a flow of $0.054 \text{ m}^3/\text{s}$, a smooth bed, a moderate relative depth of flow to the height of the hemisphere obstacle (1.85) and a bed slope of 0.00147 (experiment AS1) is used in the simulation.

The simulation is performed using a finite element mesh composed of 2780 triangular elements and 1533 nodes (Figure 5). The boundary conditions are specified as subcritical inflow, subcritical outflow and no-flow across the vertical side walls. The boundary conditions specified at the inflow section on the left are discharge intensity = $0.0443 \text{ m}^3/\text{s}/\text{m}$, $u_l = 0.0$, and $v_l = 0.0$. The boundary condition specified at the outflow section on the right is flow depth = 0.12 m. The initial depth h is set to 0.12 m. A bed slope of 0.00147 is used in the simulation. A bed roughness, k_s ,

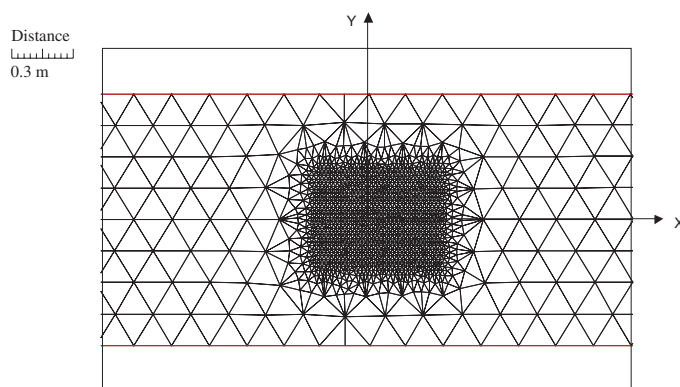


Fig. 5 Finite element mesh for Shamloo and Rajaratnam's (1997) experiment

of 0.002 m, based on a reported overall C_* of 16.5, is used. The results are shown in Figures 6-8. Figure 6 compares the experimental and numerically predicted mid-channel water surface elevation. Figures 7-8 compare the experimental and numerically predicted longitudinal velocity profiles over the vertical direction. It can be clearly seen from Figure 6 that the proposed VAM and VA models show some very small surface wave features. The experiment shows some surface disturbance but less than the models. From Figures 7-8, it can be seen that the VAM model simulates very well the longitudinal velocity profiles at different locations along the channel and give significantly better results than the De St. Venant model even for the mean flow. In particular, the wake region behind the obstacle is indicated by a relatively large u_l value, such that the bed velocity is zero.

Comparison of Computational Effort

A comparison between the VAM and the conventional De St. Venant (VA) models in terms of computational effort and time necessary for simulation is made. It is found that the time required for the VAM model to converge to a final steady state solution is approximately four times larger than that of the De St. Venant model. The memory allocated for the VAM model is found to be eleven times larger than that of the De St. Venant model, though.

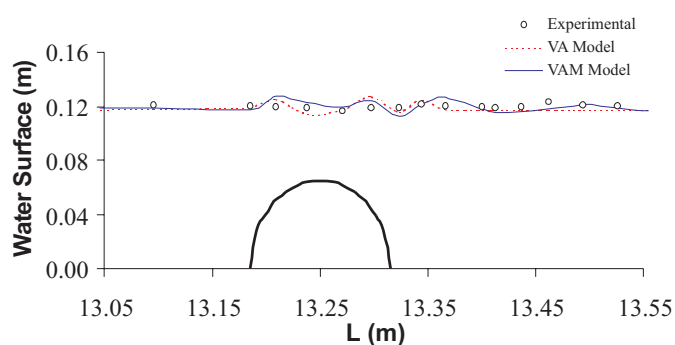


Fig. 6 The comparison of mid channel surface elevation for Shamloo and Rajaratnam's (1997) experiment

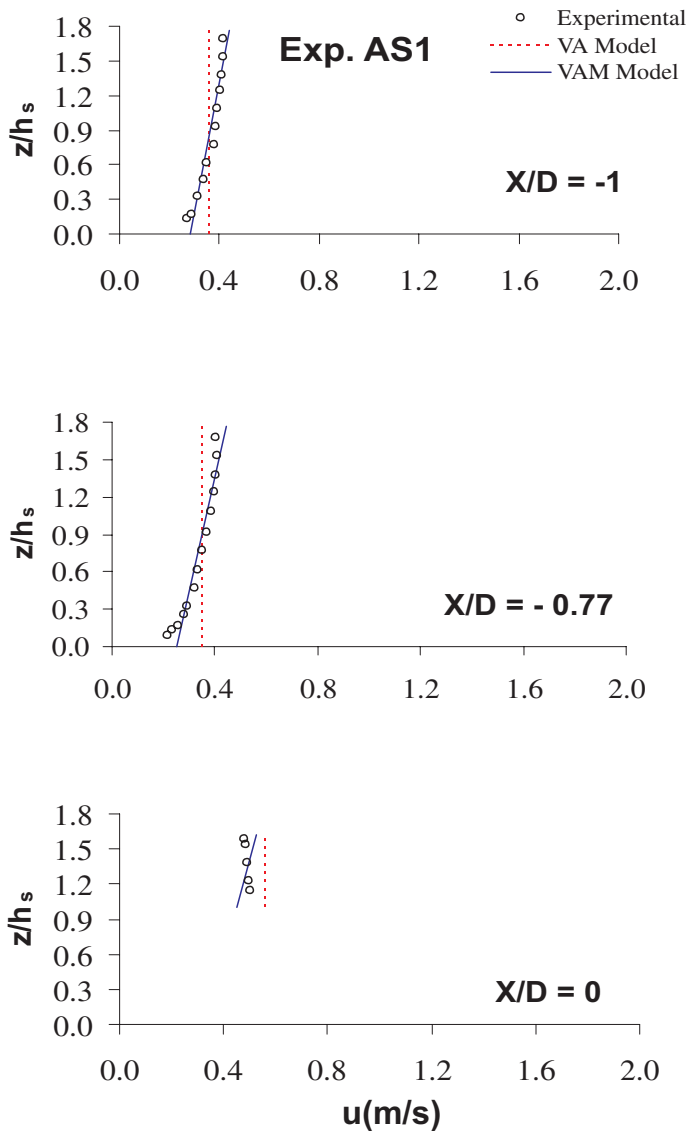


Fig. 7 The comparison of longitudinal velocity profiles along the flume for Shamloo and Rajaratnam's (1997) experiment ($X/D = -1, -0.77$ and 0)

Summary and Conclusions

The vertically averaged and moment (VAM) equations developed by Ghamry [3] were adapted to allow a pre-assumed linear distribution of the horizontal velocity components and quadratic vertical velocity and pressure distributions. The finite element hybrid Petrov-Galerkin and Standard-Galerkin schemes were used.

The obtained derived VAM equations were investigated for modeling rapidly varied flow transitions with relatively small wavelength to depth ratios ($\lambda/h \approx 5$) where non-hydrostatic pressure and non-uniform velocity distributions might be expected to be significant. Two experimental hydraulic problems from the literature were selected for comparison purposes. A comparison between the VAM 10-equation and the conventional 3-equation De St. Venant (VA) models in terms of degree of accuracy attained, computational effort and time necessary for simulation was made.

The conclusions of this study may be stated as follows:

1. Generally, a good agreement is obtained between the numerical

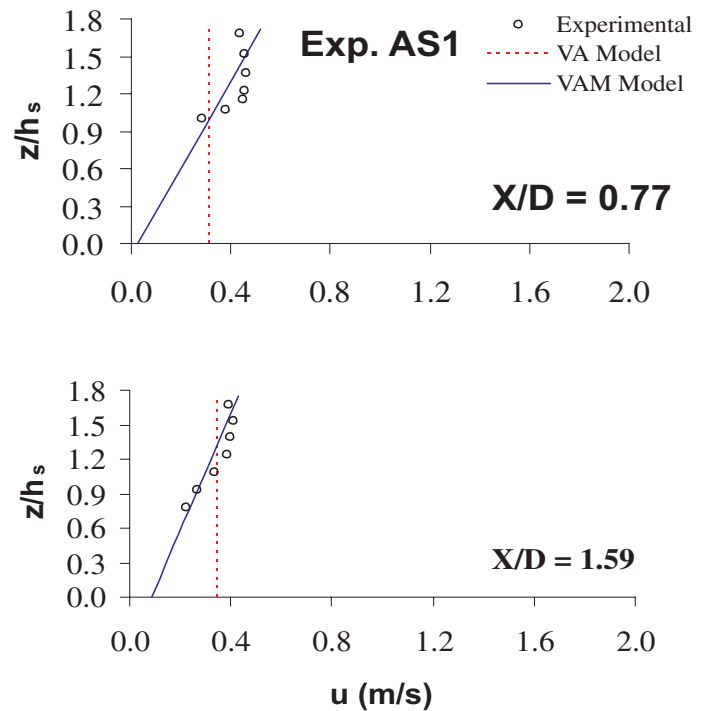


Fig. 8 The comparison of longitudinal velocity profiles along the flume for Shamloo and Rajaratnam's (1997) experiment ($X/D = 0.77$ and 1.59)

- predictions and the experimental measured data. The obtained results show that slightly improved water surface profile details are gained by the proposed model compared to the conventional depth or vertically averaged De St. Venant (VA) model.
2. Significantly better results are obtained by the proposed model than the conventional De St. Venant model in simulating and capturing the shape of the longitudinal velocity profiles over the vertical direction. The satisfactory performance of the VAM equations in these cases may be attributed to a higher degree of vertical detail incorporated in the model.
 3. It is found that the time required for the VAM model to converge to a final steady state solution is approximately four times larger than that of the traditional De St. Venant model. In addition, the memory allocated for VAM model was found to be eleven times larger than that of the De St. Venant model.

Acknowledgements

The writers would like to thank the Natural Sciences and Engineering Research Council of Canada (NSERC) for the financial support of the research, and T. Blench Hydraulics Laboratory at University of Alberta, Edmonton, which provided all the computer facilities.

Notations

- g = acceleration due to gravity;
- D = diameter of the hemisphere;
- h = depth of flow measured vertically;
- h_1 = bed pressure head in excess of hydrostatic pressure head;

h_2 = mid-depth pressure head in excess of the average of pressure heads at the bed and surface;
 h_s = $D/2$;
 k_s = effective roughness height;
 p = pressure;
 p_1 = bed pressure in excess of hydrostatic pressure;
 p_2 = mid-depth pressure in excess of the average of pressure at the bed and surface;
 q_x = discharge per unit width of the channel in x -direction;
 q_y = discharge per unit width of the channel in y -direction;
 t = time;
 u = longitudinal velocity;
 u_o = vertically averaged longitudinal velocity;
 u_1 = velocity at the surface in excess of the mean u_o ;
 u_* = shear velocity;
 v = transverse velocity;
 v_o = vertically averaged transverse velocity;
 v_1 = velocity at the surface in excess of the mean v_o ;
 w = vertical velocity;
 w_b = vertical velocity at the bed;
 \bar{w} = $1/2 w_b + 2/3 w_2 + 1/2 wh$;
 $\frac{\bar{w}}{w^2}$ = $\bar{w}^2 + \frac{w_b^2}{12} + \frac{w_h^2}{12} - \frac{w_b w_h}{6} + \frac{1}{20} (2\bar{w} - w_b - w_h)^2$;
 w_h = vertical velocity at the surface;
 w_2 = mid-depth vertical velocity in excess of the average of the vertical velocity at the bed and surface;
 x = horizontal coordinate;
 y = transverse coordinate;
 z = vertical coordinate;
 z_b = bed elevation;
 \bar{z} = mid-depth elevation = $z_b + h/2$;
 C_* = dimensionless Chezy coefficient;
VA = vertically averaged;
VAM = vertically averaged and moment;
 ν_h = eddy viscosity in x - y direction;
 ν_z = eddy viscosity in z -direction;
 \mathbf{B} = a matrix of weight functions;
 \mathbf{B} = a matrix of test functions;
 \mathbf{F}_x = a vector of x -derivative parts of the equations;
 \mathbf{F}_y = a vector of y -derivative parts of the equations;
 \mathbf{G} = a vector of non-derivative parts of the equations;
 \mathbf{W}_x = upwinding matrix in x -direction;
 \mathbf{W}_y = upwinding matrix in y -direction;
 Ψ = a vector of temporal parts of the equations;
 ϕ = vector of unknown variables at each node;
 $\tilde{\phi}$ = trial function;
 Φ = vector of nodal values of the unknown;
 Δx = discretization in the x -direction;
 Δy = discretization in the y -direction;
 η = non-dimensional vertical coordinate;
 λ = wavelength;
 ω = upwinding parameter;
 Ω = the solution domain;
 ρ = density;

$\sigma_x = \tau_{xx}$ = total turbulent normal stress in x -direction;
 $\sigma_y = \tau_{yy}$ = total turbulent normal stress in y -direction;
 $\sigma_z = \tau_{zz}$ = total turbulent normal stress in z -direction;
 $\bar{\sigma}_x = \bar{\tau}_{xx}$ = vertically averaged total turbulent normal stress in x -direction;
 $\bar{\sigma}_y = \bar{\tau}_{yy}$ = vertically averaged total turbulent normal stress in y -direction;
 $\bar{\sigma}_z = \bar{\tau}_{zz}$ = vertically averaged total turbulent normal stress in z -direction;
 $\tau_{xy} = \tau_{yx}$ = total turbulent shear stress in x - y plane;
 $\tau_{xz} = \tau_{zx}$ = total turbulent shear stress in x - z plane;
 $\tau_{yz} = \tau_{zy}$ = total turbulent shear stress in y - z plane;
 $\bar{\tau}_{xy} = \bar{\tau}_{yx}$ = vertically averaged total turbulent shear stress in x - y plane;
 $\bar{\tau}_{xz} = \bar{\tau}_{zx}$ = vertically averaged total turbulent shear stress in x - z plane;
 $\bar{\tau}_{yz} = \bar{\tau}_{zy}$ = vertically averaged total turbulent shear stress in y - z plane;
 τ_{x_b} = bed shear stress in x - z plane;
 τ_{y_b} = bed shear stress in y - z plane;

References/Bibliographic

- [1] DRESSLER, R. F. (1978), 'New Nonlinear Shallow-flow Equations with Curvature.' *Journal of Hydraulic Research*, IAHR, Vol. 16, No. 3, pp. 205-222.
- [2] FISCHER et al. (1979), 'Mixing in Inland and Coastal Waters.' Book, Academic Press, pages 21-22, Subtitle 1.4.7 Velocity Distribution in Turbulent Shear Flow.
- [3] GHAMRY, H. (1999), 'Two Dimensional Vertically Averaged and Moment Equations for Shallow Free Surface Flows.' PhD Thesis, Water Resources Engineering, Department of Civil Engineering, University of Alberta.
- [4] GHANEM, A., STEFFLER, P. M., HICKS, F. E. and KATOPODIS (1995), 'Two-Dimensional Finite Element Modeling of Flow in Aquatic Habitats'. Water resources Engineering Report No. 95-S1, Department of Civil Engineering, University of Alberta.
- [5] HENDERSON, F. M. (1966), 'Open Channel Flow.' Book, The Mcmillan Company, New York.
- [6] HICKS, F. E. and STEFFLER, P. M. (1990), 'Finite Element Modeling of Open Channel Flow.' Department of Civil Engineering, University of Alberta, Technical Report (WRE 90-6).
- [7] HICKS, F. E. and STEFFLER, P. M. (1992), 'Characteristic Dissipative Galerkin Scheme for Open-Channel Flow.' *Journal of Hydraulic Engineering*. ASCE, Vol. 118, No. 2, pp. 337-352.
- [8] HUGHES, T. J. R. and MALLET, M. (1986a), 'A new finite element formulation for computational fluid dynamics: III. The generalized streamline operator for multidimensional advective-diffusive systems.' *Computer Methods in Applied Mechanics and Engineering*, Vol. 58, pp. 305-328.
- [9] HUGHES, T. J. R. and MALLET, M. (1986b), 'A new finite element formulation for computational fluid dynamics: IV. A discontinuity-capturing operator for multidimensional

- advective-diffusive systems.' *Computer Methods in Applied Mechanics and Engineering*, Vol. 58, pp. 329-336.
- [10] HUGHES, T. J. R., MALLET, M. and MIZUKAMI, A. (1986), 'A new finite element formulation for computational fluid dynamics: II. Beyond SUPG.' *Computer Methods in Applied Mechanics and Engineering*, Vol. 54, pp. 341-355.
- [11] JIN, Y. C. and STEFFLER, P. M. (1993), 'Predicting Flow in Curved Open Channel by Depth-Averaged Method.' *Journal of Hydraulic Engineering*, ASCE, Vol. 119, No. 1, January, pp. 109-124.
- [12] JIN, Yee-Chung and LI, Baozhu (1996), 'The Use of a One-dimensional Depth-averaged Moment of Momentum Equation for the Nonhydrostatic Pressure Condition.' *Canadian Journal of Civil Engineering*, Vol. 23, pp. 150-156.
- [13] KENNEDY, J. F. (1963), 'The Mechanics of Sediment Ripples, Dunes and Antidunes in Erodible Bed Channels.' *Journal of Fluid Mechanics*, Vol. 16, Part 4, pp. 521-544.
- [14] KHAN, A. (1995), 'Modeling Rapidly Varied Open Channel Flows.' PhD Thesis, Water Resources Engineering, Department of Civil Engineering, University of Alberta.
- [15] NAEF, Daniel R. (1996), 'Extension of the 2-dimensional Shallow Water Approach Using Moment Equations.' *Proceedings of Hydroinformatics '96*, 2nd international conference, Zurich, Switzerland
- [16] ODGAARD, A. JACOB, Sinha, SANJIV K. and SOTIROPOULOS, Fotis (1998), 'Three-dimensional Numerical Model for Flow through Natural Rivers.' *Journal of Hydraulic Engineering*, ASCE, Vol. 124, No. 1, pp. 13-24.
- [17] PARSHALL, R. L. (1926), 'The improved Venturi flume.' *Trans. ASCE*, ASCE, 89, pp. 841-880.
- [18] SHAMLOO, H. and RAJARATNAM, N. (1997), 'Hydraulics of Simple Habitat Structures in Open Channels.' PhD Thesis, Water Resources Engineering, Department of Civil Engineering, University of Alberta.
- [19] SHIMUZI, Y., YAMAGUCHI, H. and ITAKURA, T. (1990), 'Three-dimensional Computation of Flow and Bed Deformation.' *Journal of Hydraulic Engineering*, ASCE, Vol. 116, No. 9, pp. 1090-1108.
- [20] STEFFLER, P. M. and JIN, Y. C. (1993), 'Depth averaged and Moment Equations for Moderately Shallow Free Surface Flow.' *Journal of Hydraulic Research*, IAHR, Vol. 31, No. 1, pp. 5-17.
- [21] YE, J. and McCORQUODALE, J. A. (1997), 'Depth-averaged hydrodynamic model in curvilinear collected grid.' *Journal of Hydraulic Engineering*, ASCE, 123(5), 380-388.

